Desalination and Water Treatment
www.deswater.com
doi: 10.5004/dwt.2020.26266

204 (2020) 257–269
November

Synthesis of xanthated chitosan beads for fast and efficient recovery of precious Ce(III) ions from aqueous solutions

Megat Ahmad Kamal Megat Hanafiah[a,b], Noorul Farhana Md Ariff[c], Shariff Ibrahim[c,*], Wan Saime Wan Ngah[d], Zurhana Mat Hussain[a]

[a]*Faculty of Applied Sciences, Universiti Teknologi MARA, 26400 Jengka, Pahang, Malaysia, emails: makmh@uitm.edu.my (M.A.K.M. Hanafiah), zurhana_mhussin@uitm.edu.my (Z.M. Hussain)*
[b]*Center of Synthesis and Chemical Biology, Institute of Science (IOS), Universiti Teknologi MARA, 40450 Shah Alam, Malaysia*
[c]*Faculty of Applied Sciences, Universiti Teknologi MARA, 40450 Shah Alam, Malaysia, emails: noorulfarhahanaariff@gmail.com (N.F. Md Ariff), sha88@uitm.edu.my (S. Ibrahim)*
[d]*School of Chemical Sciences, Universiti Sains Malaysia, 11800 Penang, Malaysia, email: wsaime@usm.my (W.S.W. Ngah)*

Received 26 September 2019; Accepted 9 June 2020

ABSTRACT

Xanthated chitosan (XC) beads, an efficient adsorbent to recover precious rare earth Ce(III) ions were prepared, characterized, and applied in this study. Factors that influence the performance in adsorption of Ce(III), which were pH of the solution, stirring rate, adsorbent dosage, and contact time, were investigated. Results revealed that the optimum conditions for adsorption of Ce(III) to be at a temperature of 300 K and pH 4, with a dosage of 0.02 g. A rapid adsorption process with only 10 min to achieve equilibrium was observed, regardless of the initial concentrations in Ce(III). Chemisorption was suggested as the rate-limiting step because of the correlation between Ce(III) adsorption process with the pseudo-second-order kinetic model. Langmuir model was found to fit well with the experimental isotherm data, and the maximum adsorption capacity of XC beads was 555.6 mg g^{-1} at 300 K. Based on the thermodynamic study, the enthalpy and entropy recorded were –6.18 kJ mol^{-1} and 130.36 J K^{-1} mol^{-1}, respectively. The nature of adsorption was exothermic as more Ce(III) ions were adsorbed at a lower temperature. Ion exchange, ionic attraction, and complexation were identified as the dominant mechanisms involved in Ce(III) adsorption.

Keywords: Adsorption; Ce(III); Xanthated chitosan; Kinetics; Isotherm

1. Introduction

In the periodic table, rare earth elements (REEs) are grouped into lanthanides series, based on the similar physical and chemical properties as well as their close electronic configuration. These elements are essential resources in various high technology industries, which include chemical engineering, information storage, energy conversion, electronic, and nuclear power industries. Cerium is one of the most abundant REEs and applied in various sectors such as steel, ceramic, catalyst, and pyrophoric alloys industries. The radioisotope from cerium is also fundamental in nuclear facilities and fission products [1–5].

Nonetheless, extensive use of REEs through mining, refining, and recycling can disrupt the ecological cycle of the environment. As such, waste management of REEs is vital and resolve any pressing environmental issues. Researches have been carried out on various methods to remove REEs from aqueous solutions, which include adsorption, membrane filtration, chemical precipitation, coagulation and flocculation, ion exchange, electrochemical treatment, and solvent extraction [2,3,6–8] to manage waste efficiently.

* Corresponding author.

However, these methods are found to have several issues such as being less effective at low concentration (<100 mg L^{-1}), generating a large amount of toxic sludge, incomplete metal removal, and being non-economic. Due to all these reasons, adsorption is thought to be the most effective treatment processes for waste management, as the adsorption does not produce sludge, is technically feasible, and effective in cost since materials are locally available [1,2,6].

The focus in adsorption is the application of biomaterials. Previous findings have found adsorption using raw chitosan record low adsorption capacity and solubility in acidic medium, which limits the application. Several modifications have been performed on chitosan, which includes introducing various functional groups or ligands to the chitosan chain [9–14]. Xanthate modification or xanthation is quite prominent as xanthate contains sulfur, which offers a strong affinity toward metal ions. Contaminants are removed while metal ions such as chitosan that originates from deacetylated chitin, are recovered. Xanthate can be synthesized by reacting with organic hydroxyl-containing biomaterial with carbon disulfide (CS_2) in a strongly alkaline solution. Modification of chitosan with xanthate is expected to enhance the adsorption performance when a new cleating group is formed on the chitosan backbone [15–17]. Chitosan exhibits good ability to adsorb metal ions due to the presence of hydroxyl (–ROH) and amino (–RNH_2) groups, apart from being abundant in nature, cheap, biodegradable, biocompatible, non-toxic, and anti-bacterial.

Raw materials, which had undergone xanthation are orange peel [6,16], activated carbon [18], de-oiled spice husk [19], sugarcane bagasse [20], rubber leaves [21], and chitosan [17,22,23]. Recently, studies have reported that the use of xanthated chitosan to remove Nd(III) produces a high amount of fast adsorption of Nd(III) [24]. However, there is still within this study, a lack of report on the mechanism of Ce(III) adsorption onto xanthated adsorbent, especially involving chitosan. Previous studies have focused on common heavy metals ions such as Zn(II), Cd(II), Cu(II), Pb(II), Ni(II), and Cr(VI) [6,16–23]. As such, the main objective of this study is to evaluate the effectiveness of xanthated chitosan (XC) beads in adsorbing Ce(III). The effects of physicochemical parameters such as pH, stirring rate, XC dosage, initial Ce(III) concentration, and contact time on adsorption of Ce(III) were investigated. The mechanisms of Ce(III) adsorption were proposed based on spectroscopic analyses, quantitative adsorption data, as well as hard and soft acids and bases (HSAB) theory.

2. Materials and methods

2.1. Materials

All chemicals in this study were analytical reagent grade and used without any purification. The Chitosan ((1,4)-2-amino-2-deoxy-beta-D-glucan) powder with 72.35% deacetylation degree was purchased from Sigma-Aldrich, Germany, while carbon disulfide, CS_2 (methanedithione) was obtained from Panreac, Spain. 2-(chloromethyl) oxirane (ECH) was bought from Merck, Germany and the cerium(III) chloride ($CeCl_3$) salt was acquired from Acros Organics, USA. Deionized water (DW) was used throughout the adsorption experiments within this study.

2.2. Preparation of XC beads

The xanthation method was adopted from a previous study [24], whereby chitosan of 2.0 g was firstly mixed with 80 mL (5%, v/v) ethanoic acid (CH_3COOH) and left overnight. The mixture was then added dropwise to 500 mL (0.50 M) NaOH solution under continuous stirring. The resulting beads were stirred at 200 rpm, with 125 mL (0.01 M) 2-(chloromethyl)oxirane (ECH) added as a crosslinking agent. The mixture was heated at 323 K and stirred for 2 h. The beads were then filtered, before being added with 50 mL (14%, w/v) NaOH and 1 mL CS_2 and left for 24 h at 300 K. The orange–red beads formed were rinsed thoroughly with DW to remove the excess base, air dried, and finally ground and sieved to obtain the size of <100 μm.

2.3. Characterization of XC beads

In determining the pH of aqueous slurry (pH_{slurry}), 1.0 g XC beads in 50 mL DW were added, stirred for 24 h, and filtered before being measured. The pH of zero-point charge (pH_{zpc}) was determined by mixing 1.0 g XC beads with 50 mL (0.01 M) KNO_3 solution in a series of beakers. Adjustment of the initial pH values was made, ranging from 4 to 12 using 0.10 M NaOH or HCl solutions, which were then left for 24 h for the final pH of the solution to be measured. The value of the pH_{ZPC} was established from the curve that cuts the pH_0 (initial pH of the solution) line of the plot ΔpH (the difference between initial pH and final pH) vs. pH_0 [25]. The energy dispersive X-ray spectrometer (EDS) was used to detect the elements present on the XC surface. The Fourier transform infrared (FTIR) spectra were obtained using an FTIR spectrophotometer (PerkinElmer 2000 Model, USA) while the surface area and average pore diameter of XC beads were identified by using a gas adsorption surface analyzer (Micromeritics ASAP 2010, USA).

2.4. Batch adsorption studies

A 1,000 mg L^{-1} Ce(III) stock solution was first prepared from $CeCl_3$ to be diluted to a concentration of 100 mg L^{-1} (unless otherwise stated) by using DW. Adsorption experiments were carried out by adding 0.01 g XC beads (unless otherwise stated) in 50 mL Ce(III) solutions using 100 mL conical flasks and stirred at 300 rpm (otherwise stated) at 300 K (room temperature). After 60 min, the mixture was filtered and analyzed for the final concentration of Ce(III) using a couple of plasma-optical emission spectrometer (ICP-OES, PerkinElmer DV5300, USA) inductively.

The effect of the initial pH for the adsorption of Ce(III) solution was investigated at pH 2–6. The pH of the solution had been adjusted by adding drops of 0.10 M HCl or NaOH solution. After adding XC, the mixture was stirred at 300 rpm for 60 min. The effect of stirring rate was observed by varying the rates from 100 to 600 rpm while the pH of Ce(III) was fixed at pH 4. A varied dosage of 0.005–0.030 g was used to observe the effects of XC dosage. In the kinetics study, 50 mL of 100, 150, and 200 mg L^{-1} Ce(III) solutions were stirred with XC beads at optimum conditions while the contact time varied from 0 to 60 min. The adsorption isotherm was determined by adding 0.02 g XC beads in 50 mL

Ce(III) solutions (100–400 mg L^{-1}) and stirred for 60 min at different temperatures (300, 310, and 320 K). The amount of Ce(III) adsorbed, q_e (mg g^{-1}), and the percentage of removal were calculated by using Eqs. (1) and (2).

$$q_e = \frac{C_0 - C_e}{m} V \tag{1}$$

$$\text{Removal}(\%) = \frac{C_0 - C_e}{C_0} \times 100 \tag{2}$$

where C_0 and C_e were the initial and equilibrium concentrations (mg L^{-1}) of Ce(III), respectively. V represented the volume of the Ce(III) solution (liter) while m was the weight of XC beads (g).

3. Results and discussion

3.1. Characterization of XC beads

The pH of zero charge (pH_{zpc}) was necessary to determine the net charge of an adsorbent. The surface charge of the adsorbent will be zero at pH = pH_{zpc}. Meanwhile, positive charges were abundant on the adsorbent surface at pH < pH_{zpc} and vice versa [26,27]. The plot for pH_{zpc} is shown in Fig. 1, and the value of pH_{zpc} for XC beads was 9.90. The pH_{zpc} value was close to the pH_{slurry} value (Table 1), indicating XC beads carried more basic groups.

The N_2 adsorption–desorption isotherm plot (Fig. S1) showed convexity towards the relative pressure axis, a characteristic of weak gas–solid interaction. This type-III isotherm behavior was usually demonstrated by microporous adsorbents [28]. The Brunauer, Emmet, and Teller (BET), as well as Langmuir surface areas, were tabulated in Table 1. Based on the table, XC was confirmed to be a nonporous adsorbent, whereby adsorption was more likely to occur at an external surface than by pore-filling mechanism.

The FTIR spectra for chitosan and XC beads (before and after Ce(III) adsorption) were compared, as shown in Fig. 2. The broad peak from 3,000 to 3,600 cm^{-1} that appeared in chitosan and XC beads spectra were attributed to N–H stretching, which overlapped with basic –OH groups. Peaks appeared at 1,595; 1,121; and 1,063 cm^{-1} in chitosan spectrum that corresponded with N–H bending vibration, an acidic C–N group that stretched vibration and symmetric stretching of C–O–C, respectively. The intensity of –OH peak in XC beads was reduced compared with chitosan beads, which indicated significant base groups –OH and $–NH_2$ converted to $–O–CS_2$ and $–NH–CS_2$, respectively. On the other hand, the peaks at 1,695; 1,595; and 1,478 cm^{-1} in XC beads were accredited to C=O, –NH bending vibrations, and C–H symmetric bends, respectively. Peaks that appeared at 1,187; 1,019; 864; and 601 cm^{-1} in XC beads spectrum corresponded to S–C–S, C=S, –O–C(S)–S, and C–S stretching vibrations.

After being loaded with Ce(III), the peaks that belonged to basic xanthate groups (1,187; 864; and 601 cm^{-1}), as well as amino (1,595 cm^{-1}) groups, either disappeared or reduced in intensity. It could be argued that Ce(III) was attached to these types of functional groups, possibly via the complexation process. In summary, the crosslinking and xanthation

Table 1
Characteristics of XC beads

Characteristics	Value
pH of aqueous slurry	9.93
pH_{zpc}	9.90
$S_{BET}{}^a$ (m^2 g^{-1})	7.96
$S_L{}^b$ (m^2 g^{-1})	10.73
$D_p{}^c$ (nm)	23.97
Beads size (μm)	<100
Color	Pale yellow

[a]BET surface area
[b]Langmuir surface area
[c]Average pore diameter

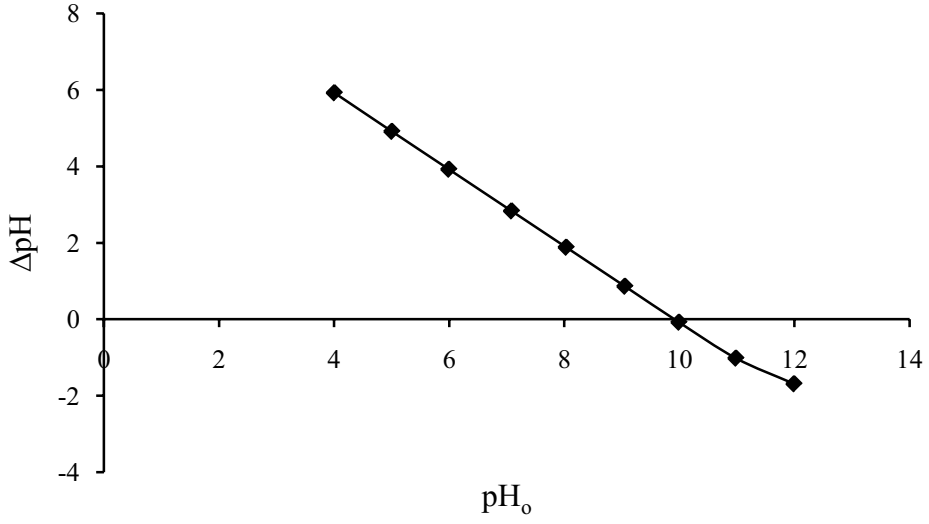

Fig. 1. Plot of pH_{zpc} of XC beads.

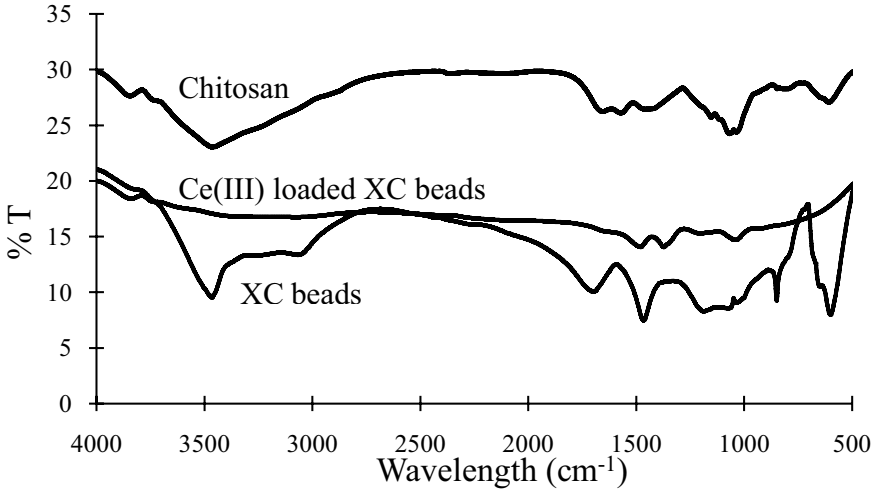

Fig. 2. FTIR spectra of chitosan, XC, and Ce(III) loaded XC beads.

reactions were represented by chemical equations shown in Fig. 3.

Fig. 4 displays the EDS spectra of XC beads before and after being loaded with Ce(III). The presence of S atom in the EDS spectra established the occurrence of the xanthation process on the XC surface. The presence of sodium ions in XC was shown at 1.1 keV.

The sodium peak disappeared after Ce(III) adsorption, which suggested that ion-exchange was involved during adsorption before Ce(III) was adsorbed. According to Dahle and Arai [29], cerium was more electronegative than sodium, with electronegativity values of 1.12 and 0.93. As electronegativity is defined as the ability of an atom to attract electrons, Ce(III) could be attracted to the sulfur atoms in XC beads by exchanging with Na^+ ions (an ion-exchange mechanism) before being adsorbed to $–CS_2$ groups via ionic attraction. Using the HSAB theory, Ce(III) ion was classified as a hard acid because of the electrons that were held tightly to the nucleus, and the ions were not easily polarised. Hard acid could form a complex with a borderline base [30], which can explain the creation of a stable complex between Ce(III) with the borderline base of the amino groups in XC beads.

3.2. Effect of pH

The pH solution was known to influence the surface charge of an adsorbent and the degree of ionization in adsorbates [31]. Since Ce(III) ions underwent hydrolysis process at pH higher than 6 [32], the effect of the initial pH of the adsorbate was studied within the range of pH 2–6. The adsorption capacity recorded at pH 2 was only 4 mg g^{-1} (Fig. S2). This low adsorption capacity was attributed to a high concentration of hydronium ions (H_3O^+), which led to a struggle of adsorption sites with adsorbates [33]. A steep increase in the adsorption capacity was observed from pH 2 to 3 with more Ce(III) ions adsorbed at pH beyond 4. Although pH 5 and 6 recorded higher adsorption capacities, Ce(III) was observed to begin precipitating at pH 5. Due to this reason, all prepared Ce(III) solutions were kept at pH 4 for subsequent adsorption studies.

3.3. Effect of stirring rate

The boundary layer surrounding the adsorbent surface could be reduced by stirring. A higher stirring rate would lead to a more rapid collision between the adsorbent and the adsorbate [34]. Thus, the stirring rate had a significant impact on the collision frequency between Ce(III) and XC surface, as shown in Fig. S3. The lowest stirring rate, which was 100 rpm resulted in 276.5 mg g^{-1} Ce(III) being adsorbed. The adsorption capacity slightly increased as the stirring rate increased, with the highest value recorded at 500 rpm. At 600 rpm, the adsorption capacity dropped somewhat to 294.4 mg g^{-1}. Hence, 500 rpm was selected as the optimum stirring rate for subsequent studies. Stirring action improved the degree of mixing and increased the concentration of Ce(III) ions near the XC surface, resulting in more Ce(III) ions to be adsorbed. A highly vigorous stirring rate, however, could lead to the desorption of adsorbates from an adsorbent surface due to the breakage of bonds [35].

3.4. Effect of XC dosage

The potential use of an adsorbent in the water treatment process could be determined from the impact of adsorbent dosage, attributed to the numbers of vacant space available for the adsorption of adsorbates [36]. In this study, the XC dosage was varied from 0.005 to 0.030 g (Fig. S4). There was a significant decrease from 526.65 to 164.09 mg g^{-1} in adsorption capacity values as the dosage increased from 0.005 to 0.030 g. The decline in adsorption capacity at higher dosages was attributed to the aggregation of adsorbent particles and the presence of more unsaturated or unadsorbed sites [37,38]. On the contrary, the removal percentage kept increasing with the increase of XC dosage and reached the maximum at 0.015 g. This condition reflected the rise in adsorption sites at higher dosages, which consequently provided more occasions to adsorb adsorbates [38,39].

3.5. Effects of initial concentration and contact time

An efficient adsorbent often shows a rapid rate of pollutant removal. The result for contact time on adsorption

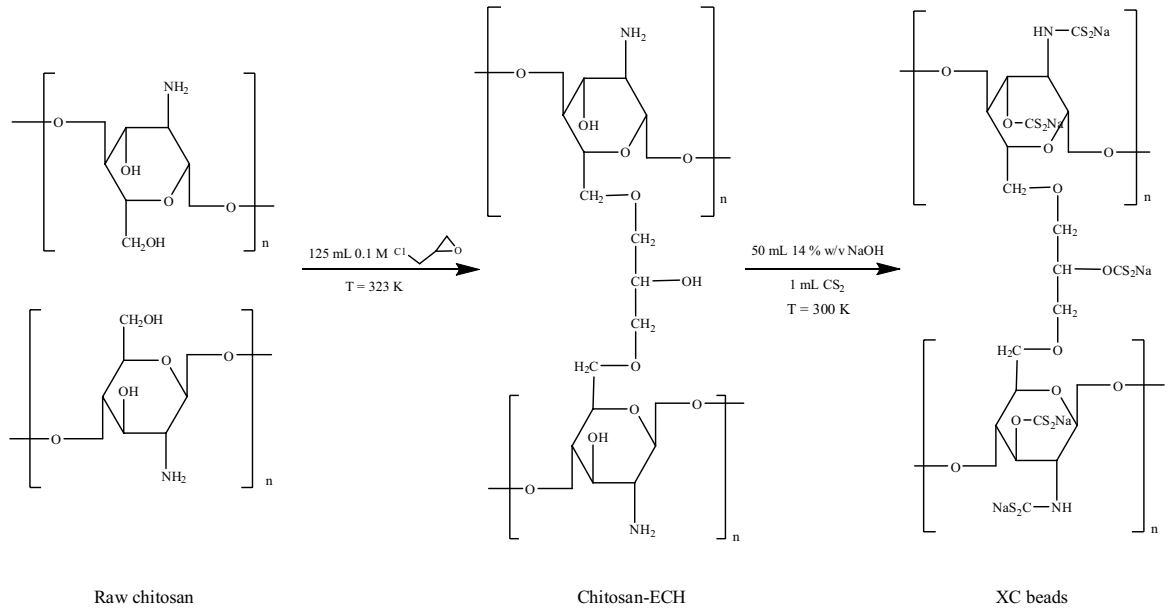

Fig. 3. Proposed synthesis of XC beads.

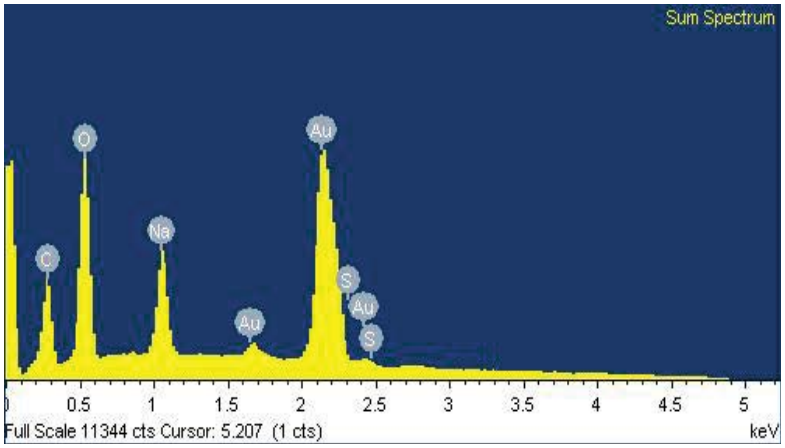

(a)

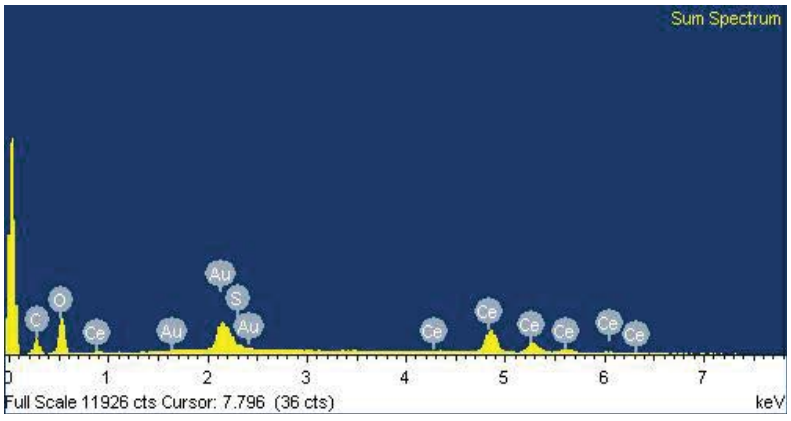

(b)

Fig. 4. EDS spectra for XC beads ((a) before adsorption of Ce(III) and (b) after adsorption of Ce(III).

of different concentrations of Ce(III) is presented in Fig. 5. Adsorption of Ce(III) on XC beads reached the equilibrium state in 5 min for all initial concentrations. The maximum adsorption capacity recorded for 100, 150, and 200 mg L^{-1} Ce(III) were 249.0, 326.2, and 496.8 mg g^{-1}, respectively. This rapid adsorption was based on the abundant active sites on the XC beads surface. Nonetheless, adsorption capacity increased as initial concentrations increased; possibly because of the extend of physical contact between metal ions and the adsorbent surface. There was also a rise in the adsorbate concentration due to diffusive mass transfer resistance [40].

3.6. Kinetics study

The kinetics data of Ce(III) adsorption on XC beads were analyzed using the pseudo-first-order and pseudo-second-order models. Both models were used widely in determining the rate of solute uptake and identifying the rate-limiting step [36]. The pseudo-first-order can be expressed as [41]:

$$\log\left(q_e - q_t\right) = \log q_e - \frac{k_1}{2.303}t \tag{3}$$

In the equation, q_e and q_t were the amount of Ce(III) adsorbed (mg g^{-1}) at equilibrium, and t was the time (min). k_1 was the pseudo-first-order rate constant (min^{-1}), which can be determined from the slope of linear plot $\log(q_e - q_t)$ against time while q_e value can be determined from the intercept of the plot. The pseudo-second-order kinetics model assumed that the adsorption process was dominated by chemisorption and adsorption of metal ions proportional to the number of active sites on the adsorbent surface. Alshameri et al. [42] suggested three steps that took place in an adsorption process. Firstly, metal ions were diffused from the liquid phase to the liquid–solid interface before being transferred to the adsorbent surface. Finally, the metal ions were diffused into particle pores. The pseudo-second-order proposed by Ho and Mckay [43] was:

$$\frac{t}{q_t} = \frac{1}{k_2 q_e^2} + \frac{1}{q_e}t \tag{4}$$

A linear plot of t/q_t vs. t could be observed if the adsorption adhered to this model. The slope of the plot provided the value of calculated adsorption at equilibrium ($1/q_{e,cal}$) while the intercept provided the value of the rate constant ($1/k_2 q_e^2$). The pseudo-first-order and pseudo-second-order plots for adsorption of Ce(III) ions onto XC beads are illustrated in Figs. S5 and S6, respectively.

Apart from observing the value of R^2, the sum of squared error (SSE) was a useful tool in determining the most fitted model, and was given as [44]:

$$\text{SSE} = \frac{\sqrt{\sum\left(q_{e,\text{exp}} - q_{e,\text{cal}}\right)^2}}{N} \tag{5}$$

The experimental and calculated adsorption capacity were $q_{e,\text{exp}}$ and $q_{e,\text{cal}}$, respectively; and N was the number of data points. Table 2 shows the summary of pseudo-first-order and pseudo-second-order rate constants calculated with experimental adsorption capacities for concentrations of 100, 150, and 200 mg L^{-1}. Pseudo-first-order model did not fit well with the adsorption data as lower correlation coefficient values were recorded compared to correlation coefficient values recorded for the pseudo-second-order model. Furthermore, higher SSE values were recorded for all Ce(III) concentrations from the pseudo-first-order model as compared to the pseudo-second-order model. In contrast, linear plots with high correlation coefficients (Table 2) were obtained by using the pseudo-second-order model. The calculated and experimental adsorption capacities were almost similar, suggesting that the adsorption of Ce(III) agreed to the pseudo-second-order model. This behavior of the uptake rate suggested the rate-limiting step during Ce(III) adsorption process was chemisorption.

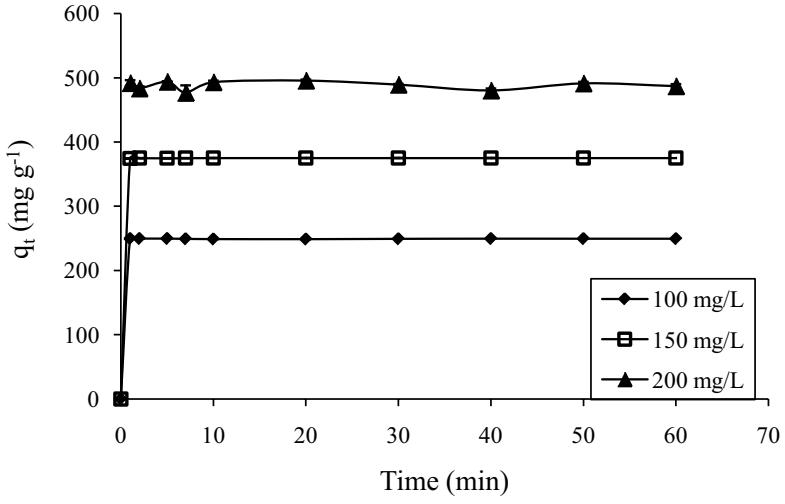

Fig. 5. Effects of initial concentrations and contact time on adsorption of Ce(III) onto XC beads (pH: 4, stirring speed: 500 rpm, adsorbent dosage: 0.02 g, and temperature 300 K).

Table 2
Comparison between pseudo-first-order, pseudo-second-order, and intraparticle diffusion rate constants calculated with experimental q_e values of 100, 150, and 200 mg L^{-1} Ce(III) onto XC beads for adsorption

[Ce(III)]	Pseudo-first-order				Pseudo-second-order			Intraparticle diffusion				
mg L^{-1}	$q_{e,cal}$ (mg g^{-1})	k_1 (min^{-1})	R^2	SSE	$q_{e,cal}$ (mg g^{-1})	k_2 (g mg^{-1} min^{-1})	R^2	SSE	k_i (mg g^{-1} $min^{-0.5}$)	C (mg g^{-1})	R^2	SSE	$q_{e,exp}$ (mg g^{-1})
100	214.8	6.91	0.998	0.008	250.0	2.02 × 10–3	1.000	2.48 × 10-8	13.90	174.3	0.2324	69.46	249.0
150	238.0	0.27	0.875	0.692	322.6	4.30 × 10–2	0.999	1.14 × 10-6	17.93	227.6	0.2280	90.73	326.2
200	229.6	1.55	0.785	0.841	495.8	1.20 × 10–1	0.999	1.19 × 10-6	26.66	344.9	0.2212	137.6	496.8

The intraparticle diffusion equation was given in the following equation:

$$q_t = k_i t^{\frac{1}{2}} + C \tag{6}$$

In the equation, q_t was the adsorption capacity (mg g^{-1}) at the time (t) in min while k_i was the intraparticle rate constant (mg g^{-1} $min^{-0.5}$), and C was the thickness of a boundary layer (mg g^{-1}). A linear plot of q_t against the square root of time, $t^{1/2}$, may give information of the intraparticle constant, k_i (mg g^{-1} $min^{-0.5}$) from the slope, and the thickness of the boundary layer for the adsorbent through the intercept of the plot. If the value of the intercept were zero (C=0), the adsorption rate-limiting step would be controlled solely by the diffusion mechanism. However, if the intercept did not go through the origin (C≠0), the adsorption process might be contributed by other mechanisms, alongside intraparticle diffusion [45–49]. The deviation of experimental data from the intraparticle diffusion kinetic model indicated that the film diffusion process had dominated the adsorption of Ce(III) onto XC beads, which illustrated the entire rate of the adsorption process [50,51]. The intercept of intraparticle diffusion plots for adsorption of Ce(III) ions onto XC beads were not equal to zero (C≠0), where the values recorded for the system ranged from 174.3 to 344.9 mg g^{-1}. The non-zero values of C indicated that the adsorption mechanism was not controlled solely by the intraparticle diffusion mechanism, but may have been governed by other mechanisms [51]. In Table 2, the value of C given describes the amount of Ce(III) ions being adsorbed onto XC beads through film diffusion, such as the more significant the value of C, the more ions would be adsorbed through film diffusion [51].

3.7. Adsorption isotherms

The adsorption isotherm was a relationship between the amount of Ce(III) adsorbed per unit weight of XC beads and the concentration of Ce(III) in bulk solution. In this study, the adsorption isotherm study was carried out at three different temperatures, and the results are shown in Fig. 6.

Based on the Giles isotherm classification system, the shapes of the isotherm plots for adsorption of Ce(III) fall into type "H2", which indicated the strong affinity of the solute–solution system, typically shaped in chemisorption [52]. Adsorption of Ce(III) however, decreased with an increase in temperature, whereby the maximum adsorption capacities at 300, 310, and 320 K were 555.6, 500.0, and 476.2 mg g^{-1}, respectively. Two most common isotherm models, the Langmuir and Freundlich models, were used to describe this data.

The linearized Langmuir equation was [53]:

$$\frac{C_e}{q_e} = \frac{1}{Q_{max} b} + \frac{C_e}{Q_{max}} \tag{7}$$

where C_e was the equilibrium Ce(III) concentration (mg L^{-1}), while q_e was the amount of Ce(III) adsorbed at equilibrium (mg g^{-1}). Q_{max} was the maximum adsorption capacity (mg g^{-1}), and b was the constant (L mg^{-1}). The value of b reflected the

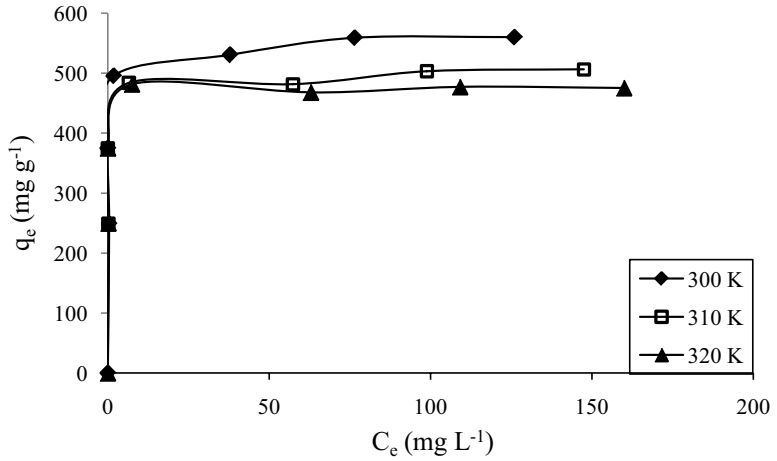

Fig. 6. Adsorption isotherm plot of Ce(III) adsorption at 300, 310, and 320 K (pH: 4, stirring speed: 500 rpm, adsorbent dosage: 0.02 g, and contact time: 30 min).

binding strength between Ce(III) and XC surface. On the other hand, the Freundlich model was expressed as:

$$\log q_e = \log K_F + \frac{1}{n}\log C_e \quad (8)$$

where K_F represented the Freundlich constant (mg g^{-1}), while n was considered to be the heterogeneity of the adsorbent surface and its affinity for the adsorbate. Based on Table 3, higher correlation coefficient values (R^2) were recorded for the Langmuir isotherm model compared to the Freundlich isotherm model for all temperatures. Also, lower SSE values were recorded for the Langmuir model, which can conclude that Ce(III) adsorption process adhered to the Langmuir model, whereby the adsorption was monolayer and occurred at similar energy sites [54]. The n values obtained from the Freundlich isotherm model were higher than the accord of all temperatures, further indicating that there was a strong bond between adsorbent and adsorbates [53]. The performance of XC beads in recovering Ce(III) was compared with other adsorbents, and their respective adsorption capacities are summarized in Table 4.

3.8. Adsorption thermodynamic

The value of enthalpy change ($\Delta H°$) was important in determining whether the adsorption was endothermic or exothermic. Values from $\Delta G°$ and $\Delta S°$ could explain the spontaneity of adsorption as well as the attraction between adsorbent and adsorbates. The following equations were used to obtain the thermodynamic parameters [60]:

$$\ln b = \frac{\Delta S°}{R} - \frac{\Delta H°}{RT} \quad (9)$$

$$\Delta G° = -RT\ln b \quad (10)$$

In these equations, b represented the Langmuir constant (L mol^{-1}), while R represented the gas constant (8.314 J K^{-1} mol^{-1}). $\Delta H°$ was the enthalpy change (kJ mol^{-1}), while $\Delta S°$ was an entropy change (J K^{-1} mol^{-1}) and $\Delta G°$ was the Gibbs free energy (kJ mol^{-1}) used. T represented the temperature in Kelvin. Eq. (9) was used to obtain the Van't Hoff plot. The values of enthalpy change ($\Delta H°$) and entropy change ($\Delta S°$) can be obtained from the slope and intercept of ln$b$ vs. 1/T. Based on Van't Hoff plot (Fig. 7), the values obtained for entropy change ($\Delta S°$) and enthalpy change ($\Delta H°$) were 130.36 J K^{-1} mol^{-1} and –6.18 kJ mol^{-1}, respectively (Table 5). A positive value of $\Delta S°$ change depicted an increased disorder at the solid–liquid interface during Ce(III) adsorption. The negative value of $\Delta H°$ change indicated that the adsorption process was naturally exothermic. However, a considerably low value of $\Delta H°$ could also be explained as physical adsorption of Ce(III) onto XC beads with a weak interaction between adsorbent and adsorbate [61].

Nonetheless, all the values of Gibb's free energy were negative, indicating a spontaneous nature of Ce(III)

Table 3
Langmuir and Freundlich parameters for adsorption of Ce(III) onto XC beads at 300, 310, and 320 K

Temperature (K)	Langmuir			Freundlich				
	Q_{max} (mg g^{-1})	b (L mg^{-1})	R^2	SSE	K_F (mg g^{-1})	n	R^2	SSE
300	555.6	1.2	0.999	2.37×10^{-6}	342.8	8.60	0.481	8.19×10^{-3}
310	500.0	1.7	0.999	6.28×10^{-6}	382.0	17.3	0.575	5.00×10^{-3}
320	476.2	7.0	0.999	7.85×10^{-7}	374.0	18.7	0.562	4.70×10^{-3}

Table 4
Comparison of maximum adsorption capacity (Q_{max}) value for adsorption of Ce(III) onto various types of adsorbents

Adsorbents	Q_{max} (mg g^{-1})	References
XC beads	555.6	This study
Poly(acrylic acid) brushes-decorated attapulgite	295.4	[32]
Activated carbon-based amino phosphonic acid chelating resin	94.3	[55]
Hybrid nano-material	130.0	[56]
Poly(allylamine)/silica composite	111.8	[57]
Monosodium glutamate functionalized chitosan	369.0	[58]
Yeast/silica composite	36.1	[59]

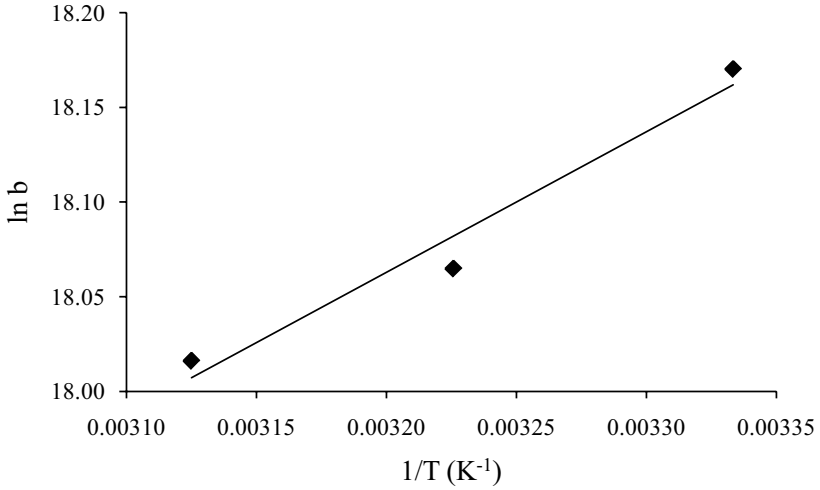

Fig. 7. Van't Hoff plot for adsorption of Ce(III) onto XC beads.

Table 5
Thermodynamic parameters for adsorption of Ce(III) onto XC beads

Temperature (K)	$\Delta G°$ (kJ mol^{-1})	$\Delta H°$ (kJ mol^{-1})	$\Delta S°$ (J K^{-1} mol^{-1})
300	–45.32	–6.18	130.36
310	–46.56		
320	–47.93		

adsorption. The decrease in $\Delta G°$ values suggested a decline in the spontaneity of the adsorption process, where the energy to overcome the barrier for the adsorption process was reduced at higher temperature [62]. The reduction of Ce(III) adsorption at higher temperatures can be explained by the increase in the tendency of adsorbed Ce(III) ions to escape from XC beads based on the rise in the total energy of the solution, as well as deactivation of some functional groups on the adsorbent [51].

4. Conclusion

This study demonstrates a potential application of XC beads for recovery of precious Ce(III) ions from aqueous solutions. In characterization studies, the XC beads carried more basic groups as the pH slurry and pH_{zpc} values were 9.90 and 9.93, respectively. Results from the BET and Langmuir surface areas confirmed that XC beads were non-porous and Ce(III) ions adsorption most likely occurred at the external surface. In the FTIR spectra, the disappearance of basic xanthate groups (1,187; 864; and 601 cm^{-1}), as well as amino (1,595 cm^{-1}) groups confirmed the adsorption of Ce(III) ions on these groups. The efficiency of the adsorption process was found to be dependent on physicochemical factors such as pH, stirring rate, and XC dosage. The maximum adsorption capacity of Ce(III) ions was observed at pH 4, stirring speed of 500 rpm, and XC beads dosage of 0.02 g. Meanwhile, based on the kinetics study, adsorption of Ce(III) ions agreed well to the pseudo-second-order model than the pseudo-first-order, which suggests that chemisorption is a rate-limiting step. The maximum adsorption capacity that has been recorded in this study using the Langmuir isotherm model is 555.6 mg g^{-1} at 300 K. The nature of adsorption was exothermic with the enthalpy and entropy recorded were –6.18 kJ mol^{-1} and 130.36 J K^{-1} mol^{-1}, respectively. Ion-exchange reactions occur between Ce(III) and Na^+ ions due to the electronegativity effect. Formation of complexes between amino groups and Ce(III) ions has been explained based on the hard acid and hard base interaction. Overall, this study demonstrates that xanthation is an effective method to adsorb Ce(III) ions as a high adsorption capacity and a fast rate of uptake were noticed. However, the

use of CS2, a very toxic chemical could generate a secondary pollution problem.

Acknowledgments

The authors are grateful to the Malaysian Ministry of Education for financial support under the Fundamental Research Grant Scheme (FRGS), vote no. 600-RMI/FRGS 5/3 (1/2012), and Bestari Perdana Grant Scheme, Universiti Teknologi MARA, vote No. 600-IRMI/PERDANA 5/3 BESTARI (037/2018).

References

[1] M. Torab-Mostaedi, Biosorption of lanthanum and cerium from aqueous solutions using tangerine (*Citrus reticulata*) peel: equilibrium, kinetic, and thermodynamic studies, Chem. Ind. Chem. Eng. Q., 19 (2013) 79–88.
[2] A.A. Galhoum, M.G. Mahfouz, S.T. Abdel-Rehem, N.A. Gomaa, A.A. Atia, T. Vincent, E. Guibal, Diethylenetriamine-functionalized chitosan magnetic nano-based particles for the sorption of rare earth metal ions [Nd(III), Dy(III) and Yb(III)], Cellulose, 22 (2015) 2589–2605.
[3] Y. Zhu, Y. Zheng, A. Wang, A simple approach to fabricate granular adsorbent for adsorption of rare elements, Int. J. Biol. Macromol., 72 (2015) 410–420.
[4] H. Faghihian, M.K. Amini, A.R. Nezamzadeh, Cerium uptake by zeolite A synthesized from natural clinoptilolite tuffs, J. Radioanal. Nucl. Chem., 264 (2005) 577–582.
[5] M.R. Awual, T. Yaita, H. Shiwaku, Design a novel optical adsorbent for simultaneous ultra-trace cerium(III) detection, sorption and recovery, Chem. Eng. J., 228 (2013) 327–335.
[6] S. Liang, X. Guo, N. Feng, Q. Tian, Application of orange peel xanthate for the adsorption of Pb^{2+} from aqueous solutions, J. Hazard. Mater., 170 (2009) 425–429.
[7] S. Zafar, M. Khan, M. Khraisheh, S. Shahida, T. Javed, M.L. Mirza, N. Khalid, Use of rice husk as an effective sorbent for the removal of cerium ions from aqueous solution: kinetic, equilibrium and thermodynamic studies, Desal. Water Treat., 150 (2019) 124–165.
[8] J.Y. Yang, B.Y. Yue, J. Teng, Q. Liu, X.Y. Jiang, M. Zhong, F.L. Zhou, J.G. Yu, Dichlorocarbene modified graphene oxide nanocomposite fabricated by a facile hydrothermal method and its adsorption properties toward rare earth elements, Desal. Water Treat., 162 (2019) 260–268.
[9] X. Jiang, Y. Sun, L. Liu, S. Wang, X. Tian, Adsorption of C.I. Reactive Blue 19 from aqueous solutions by porous particles of the grafted chitosan, Chem. Eng. J., 235 (2014) 151–157.
[10] L. Zhang, X. Liu, W. Xia, W. Zhang, Preparation and characterization of chitosan-zirconium(IV) composite for adsorption of vanadium(V), Int. J. Biol. Macromol., 64 (2014) 155–161.
[11] L.C. Zhou, X.G. Meng, J.W. Fu, Y.C. Yang, P. Yang, C. Mi, Highly efficient adsorption of chlorophenols onto chemically modified chitosan, Appl. Surf. Sci., 292 (2014) 735–741.
[12] J. Maity, S.K. Ray, Enhanced adsorption of methyl violet and congo red by using semi and full IPN of polymethacrylic acid and chitosan, Carbohydr. Polym., 104 (2014) 8–16.
[13] J. Wang, L. Wang, H. Yu, Y. Chen, Q. Chen, W. Zhou, H. Zhang, X. Chen, Recent progress on synthesis, property and application of modified chitosan: an overview, Int. J. Biol. Macromol., 88 (2016) 333–344.
[14] C. Lee, H. Lin, E.I. Cadogan, S.R. Popuri, C. Chang, Biosorption performance of biodegradable polymer powders for the removal of gallium(III) ions from aqueous solution, Pol. J. Chem. Technol., 17 (2015) 124–132.
[15] D. Chauhan, N. Sankararamakrishnan, Highly enhanced adsorption for decontamination of lead ions from battery wastewaters using chitosan functionalized with xanthate, Bioresour. Technol., 99 (2008) 9021–9024.
[16] S. Liang, X. Guo, N. Feng, Q. Tian, Effective removal of heavy metals from aqueous solutions by orange peel xanthate, Trans. Nonferrous Met. Soc. China, 20 (2010) S187–S191.
[17] N. Sankararamakrishnan, A. Dixit, L. Iyengar, R. Sanghi, Removal of hexavalent chromium using a novel cross linked xanthated chitosan, Bioresour. Technol., 97 (2006) 2377–2382.
[18] A. Behnamfard, M.M. Salarirad, F. Vegliò, Removal of Zn(II) ions from aqueous solutions by ethyl xanthate impregnated activated carbons, Hydrometallurgy, 144–145 (2014) 39–53.
[19] T. Torres-Blancas, G. Roa-Morales, C. Fall, C. Barrera-Díaz, F. Ureña-Nuñez, T.B. Pavón Silva, Improving lead sorption through chemical modification of de-oiled allspice husk by xanthate, Fuel, 110 (2013) 4–11.
[20] P. Lal Homagai, K.N. Ghimire, K. Inoue, Adsorption behavior of heavy metals onto chemically modified sugarcane bagasse, Bioresour. Technol., 101 (2010) 2067–2069.
[21] W.K.A.W. Khalir,M.A.K.M. Hanafiah,S.Z.M. So'ad, W.S.W. Ngah, Adsorption behavior of Pb(II) onto xanthated rubber (*Hevea brasiliensis*) leaf powder, Pol. J. Chem. Technol., 13 (2011) 84–88.
[22] B. Kannamba, K.L. Reddy, B.V. AppaRao, Removal of Cu(II) from aqueous solutions using chemically modified chitosan, J. Hazard. Mater., 175 (2010) 939–948.
[23] S.P. Kuang, Z.Z. Wang, J. Liu, Z.C. Wu, Preparation of triethylenetetramine grafted magnetic chitosan for adsorption of Pb(II) ion from aqueous solutions, J. Hazard. Mater., 260 (2013) 210–219.
[24] N.F.M. Ariff, M.A.K. Megat Hanafiah, Z.M. Hussin, S.C. Ibrahim, W.S.W. Ngah, Kinetics and isotherm studies on Nd(III) adsorption onto xanthated chitosan, Mater. Sci. Forum, 857 (2016) 530–534.
[25] W.S. Wan Ngah, M.A.K.M. Hanafiah, Biosorption of Cu(II) ions from dilute aqueous solutions on base treated rubber (*Hevea brasiliensis*) leaves powder: kinetics, isotherm, and biosorption mechanisms, J. Environ. Sci., 20 (2008) 1168–1176.
[26] W.S. Wan Ngah, M.A.K.M. Hanafiah, Adsorption of copper on rubber (*Hevea brasiliensis*) leaf powder: kinetic, equilibrium and thermodynamic studies, Biochem. Eng. J., 39 (2008) 521–530.
[27] L. Monser, N. Adhoum, Tartrazine modified activated carbon for the removal of Pb(II), Cd(II) and Cr(III), J. Hazard. Mater., 161 (2009) 263–269.
[28] K.S.W. Sing, Reporting gas adsorption data for gas/solid system with special reference to the determination of surface area and porosity, Pure Appl. Chem., 54 (1982) 2201–2218.
[29] J.T. Dahle, Y. Arai, Applications and toxicology of cerium oxide nanoparticles, Int. J. Environ. Res. Public Health, 12 (2015) 1253–1278.
[30] E. Nieboer, D.H.S. Richardson, The replacement of the nondescript term 'heavy metals' by a biologically and chemically significant classification of metal ion, Environ. Pollut., 1 (1980) 3–26.
[31] M.R. Fathi, A. Asfaram, A.Farhangi, Removal of Direct Red 23 from aqueous solution using corn stalks: isotherms, kinetics and thermodynamic studies, Spectrochim. Acta, Part A, 135C (2014) 364–372.
[32] X.J. Li, C.J. Yan, W.J. Luo, Q. Gao, Q. Zhou, C. Liu, S. Zhou, Exceptional cerium(III) adsorption performance of poly(acrylic acid) brushes-decorated attapulgite with abundant and highly accessible binding sites, Chem. Eng. J., 284 (2016) 333–342.
[33] M.J.C. Calagui, D.B. Senoro, C.C. Kan, J.W.L. Salvacion, C.M. Futalan, M.W. Wan, Adsorption of indium(III) ions from aqueous solution using chitosan-coated bentonite beads., J. Hazard. Mater., 277 (2014) 120–126.
[34] W.S. Wan Ngah, L.C. Teong, M.A.K.M. Hanafiah, Adsorption of dyes and heavy metal ions by chitosan composites: a review, Carbohydr. Polym., 83 (2011) 1446–1456.
[35] M.E. Argun, S. Dursun, C. Ozdemir, M. Karatas, Heavy metal adsorption by modified oak sawdust: thermodynamics and kinetics, J. Hazard. Mater., 141 (2007) 77–85.
[36] B. Sarada, M.K. Prasad, K.K. Kumar,C.V.M. Ramachandra, Cadmium removal by macro algae *Caulerpa fastigiata*: characterization, kinetic, isotherm and thermodynamic studies, J. Environ. Chem. Eng., 2 (2014) 1533–1542.

[37] Y. Jiang, H. Pang, B. Liao, Removal of copper(II) ions from aqueous solution by modified bagasse, J. Hazard. Mater., 164 (2009) 1–9.
[38] W. Pitakpoolsil, M. Hunsom, Adsorption of pollutants from biodiesel wastewater using chitosan flakes, J. Taiwan Inst. Chem. Eng., 44 (2013) 963–971.
[39] E. Alver, A.Ü. Metin, Anionic dye removal from aqueous solutions using modified zeolite: adsorption kinetics and isotherm studies, Chem. Eng. J., 200–202 (2012) 59–67.
[40] A. Hassani, F. Vafaei, S. Karaca, A.R. Khataee, Adsorption of a cationic dye from aqueous solution using Turkish lignite: Kinetic, isotherm, thermodynamic studies and neural network modeling, J. Ind. Eng. Chem., 20 (2014) 2615–2624.
[41] Y.S. Ho, G. McKay, A comparison of chemisorption kinetic models applied to pollutant removal on various sorbents, Saf. Environ. Prot., 76 (1998) 332–340.
[42] A. Alshameri, C. Yan, Y. Al-Ani, A.S. Dawood, A. Ibrahim, C. Zhou, H. Wang, An investigation into the adsorption removal of ammonium by salt activated Chinese (Hulaodu) natural zeolite: kinetics, isotherms, and thermodynamics, J. Taiwan Inst. Chem. Eng., 45 (2014) 554–564.
[43] Y.S. Ho, G. McKay, The kinetics of sorption of divalent metal ions onto sphagnum moss peat, Water Res., 34 (2000) 735–742.
[44] G. Huang, C. Yang, K. Zhang, J. Shi, Adsorptive removal of copper ions from aqueous solution using cross-linked magnetic chitosan beads, Chin. J. Chem. Eng., 17 (2009) 960–966.
[45] M.T. Yagub, T.K. Sen, S. Afroze, H.M. Ang, Dye and its removal from aqueous solution by adsorption: a review, Adv. Colloid Interface Sci., 209 (2014) 172–184.
[46] B. Yu, J. Xu, J.H. Liu, S.T. Yang, J. Luo, Q. Zhou, J. Wan, R. Liao, H. Wang, Y. Liu, Adsorption behavior of copper ions on graphene oxide–chitosan aerogel, J. Environ. Chem. Eng., 1 (2013) 1044–1050.
[47] A.S.K. Krishna, S.J. Jiang, Chitosan-functionalized graphene oxide: a novel adsorbent an efficient adsorption of arsenic from aqueous solution, J. Environ. Chem. Eng., 4 (2016) 1698–1713.
[48] T.C. Sarat, S.N. Mudliar, S. Vidyashankar, S. Mukherji, R. Sarada, K. Krishnamurthi, V.S. Chauhan, Defatted algal biomass as a non-conventional low-cost adsorbent: surface characterization and methylene blue adsorption characteristics, Bioresour. Technol., 184 (2015) 395–404.
[49] M.J. Ahmed, S.K. Dhedan, Equilibrium isotherms and kinetics modeling of methylene blue adsorption on agricultural wastes-based activated carbons, Fluid Phase Equilib., 317 (2012) 9–14.
[50] P.K. Gautam, R.K. Gautam, S. Banerjee, G. Lofrano, M.A. Sanroman, M.C. Chattopadhyaya, J.D. Pandey, Preparation of activated carbon from Alligator weed (*Alternenthera philoxeroids*) and its application for tartrazine removal: isotherm, kinetics and spectroscopic analysis, J. Environ. Chem. Eng., 3 (2015) 2560–2568.
[51] M.R. Prasanthi, M. Jayasravanthi, R.V. Nadh, Kinetic, isotherm and thermodynamics investigation on adsorption of divalent copper using agro-waste biomaterials, *Musa acuminata*, *Casuarina equisetifolia* L. and *Sorghum bicolor*, Pol. J. Chem. Technol., 18 (2016) 68–77.
[52] C.H. Giles, D. Smith, A. Huitson, A general treatment and classification of the solute adsorption isotherm, J. Colloid Interface Sci., 47 (1974) 755–765.
[53] W.S. Wan Ngah, N.F.M. Ariff, A. Hashim, M.A.K.M. Hanafiah, Malachite green adsorption onto chitosan coated bentonite beads: isotherms, kinetics and mechanism, Clean Soil Air Water, 38 (2010) 394–400.
[54] J.J. Chen, A.L. Ahmad, B.S. Ooi, Poly(N-isopropylacrylamide-co-acrylic acid) hydrogels for copper ion adsorption: equilibrium isotherms, kinetic and thermodynamic studies, J. Environ. Chem. Eng., 1 (2013) 339–348.
[55] T. Chen, C. Yan, Y. Wang, C. Tang, S. Zhou, Y. Zhao, R. Ma, P. Duan, Synthesis of activated carbon-based amino phosphonic acid chelating resin and its adsorption properties for Ce(III) removal, Environ. Technol., 36 (2015) 2168–2176.
[56] T. Yousefi, S. Yavarpour, S.H. Mousavi, M. Torab-Mostaedi, R. Davarkhah, H.G. Mobtaker, Effective removal of Ce(III) and Pb(II) by new hybrid nano-material: $H_yPM_{o12}O_{40}$@$Fe(III)_x$ $Sn(II)_y Sn(IV)_{1-x-y}$, Process Saf. Environ. Prot., 98 (2015) 211–220.
[57] S. Zhou, X. Li, Y. Shi, A. Alshameri, C. Yan, Preparation, characterization, and Ce(III) adsorption performance of poly(allylamine)/silica composite, Desal. Water Treat., 56 (2015) 1321–1334.
[58] M.A.K.M. Hanafiah, Z.M. Hussin, N.F.M. Ariff, W.S.W. Ngah, S.C. Ibrahim, Monosodium glutamate functionalized chitosan beads for adsorption of precious cerium ion, Adv. Mater. Res., 970 (2014) 198–203.
[59] W. Huang, Y. Song, H. Ou, W. Bian, J. Pan, Adsorption behavior and mechanism of Ce(III) on yeast/silica composite, Nat. Sci. Ed., 34 (2013) 212–216.
[60] T.S. Anirudhan, P.G. Radhakrishnan, Thermodynamics and kinetics of adsorption of Cu(II) from aqueous solutions onto a new cation exchanger derived from tamarind fruit shell, J. Chem. Thermodyn., 40 (2008) 702–709.
[61] T.A. Khan, S.A. Chaudhry, I. Ali, Equilibrium uptake, isotherm and kinetic studies of Cd(II) adsorption onto iron oxide activated red mud from aqueous solution, J. Mol. Liq., 202 (2015) 165–175.
[62] J. Liu, L. Wan, L. Zhang, Q. Zhou, Effect of pH, ionic strength, and temperature on the phosphate adsorption onto lanthanum-doped activated carbon fiber, J. Colloid Interface Sci., 364 (2011) 490–496.

Supplementary information

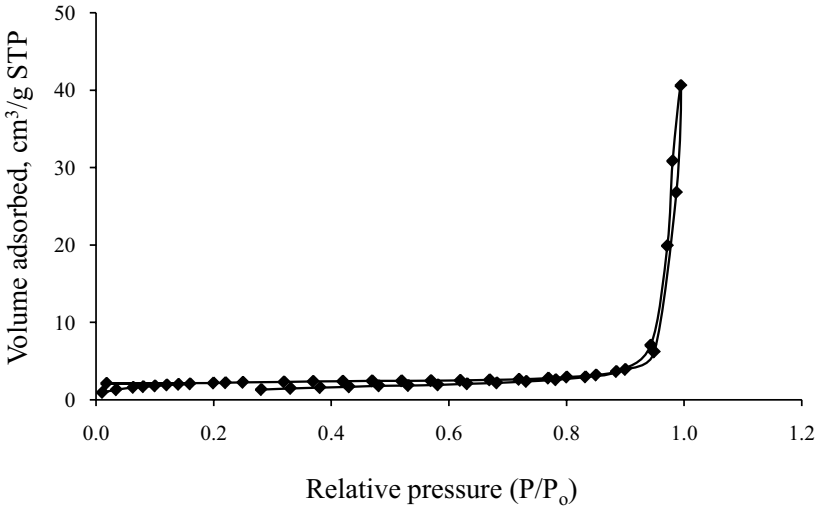

Fig. S1. N_2 adsorption–desorption isotherm plot of XC beads.

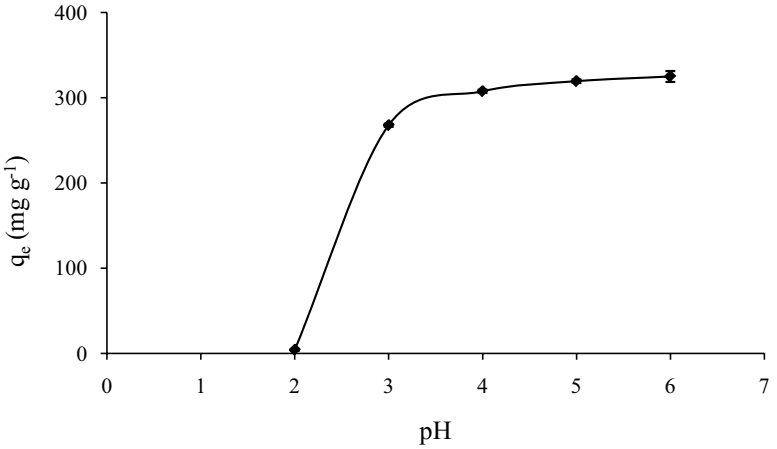

Fig. S2. Effect of initial pH on adsorption of Ce(III) onto XC beads (stirring speed: 300 rpm, adsorbent dosage: 0.01 g, stirring time: 30 min, and temperature 300 K).

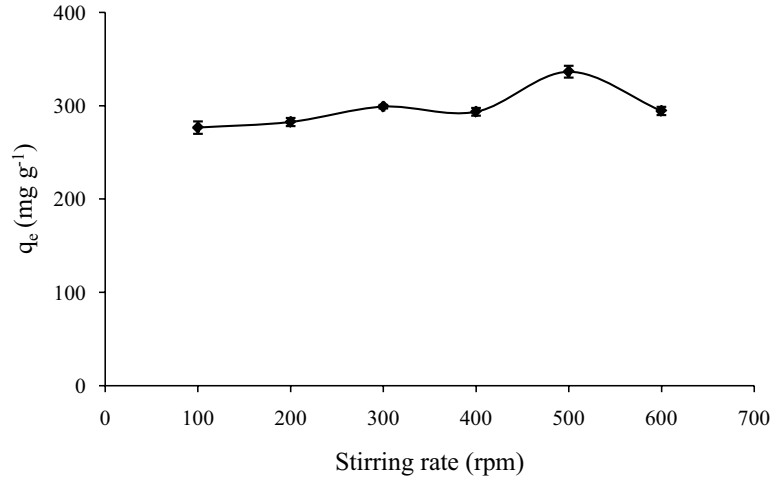

Fig. S3. Effect of stirring rate on adsorption of Ce(III) onto XC beads (pH: 4, adsorbent dosage: 0.01 g, stirring time: 30 min, and temperature 300 K).

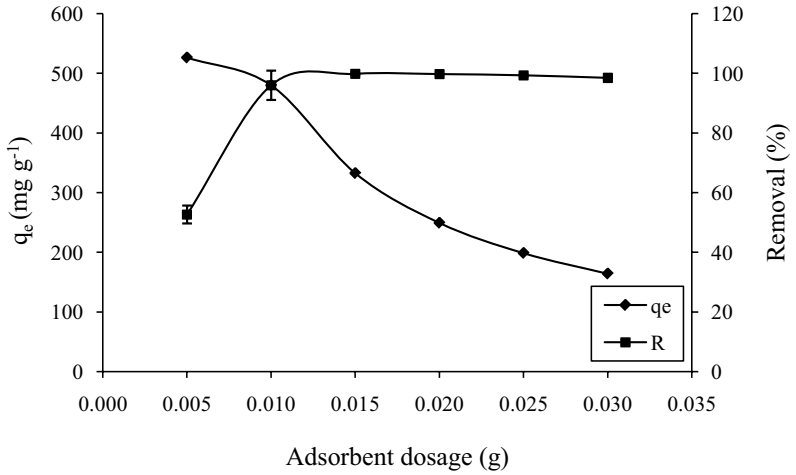

Fig. S4. Effect of adsorbent dosage on adsorption of Ce(III) onto XC beads (pH: 4, stirring speed: 500 rpm, stirring time: 30 min, and temperature 300 K).

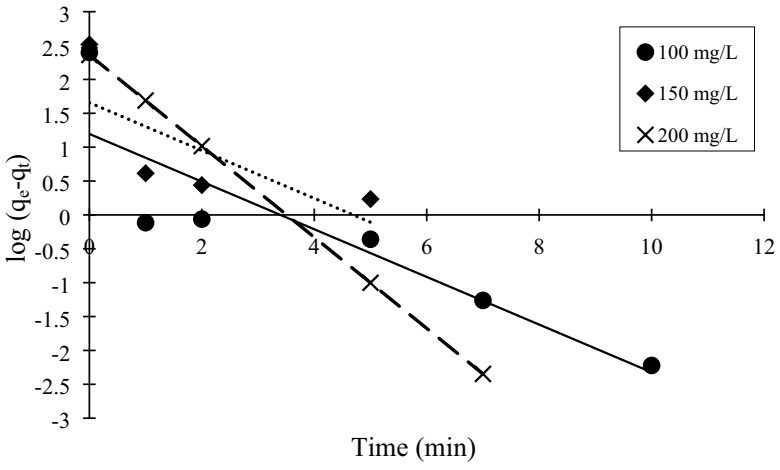

Fig. S5. Pseudo-first-order model for adsorption of 100, 150, and 200 mg L^{-1} Ce(III) ions onto XC beads at 300 K.

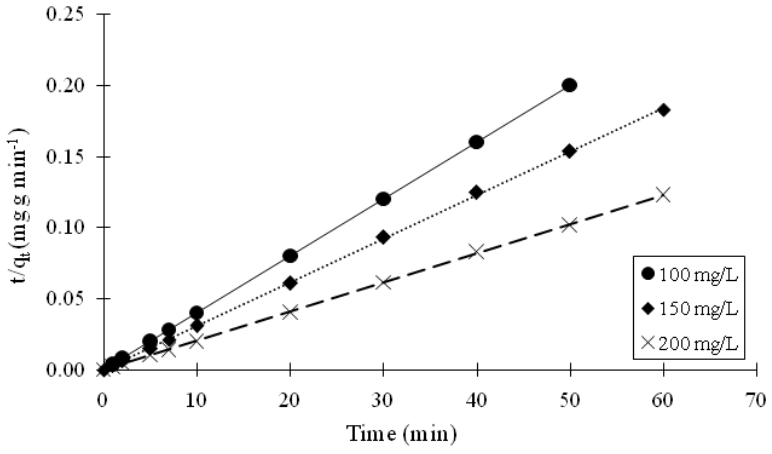

Fig. S6. Pseudo-second-order model for adsorption of 100, 150, and 200 mg L^{-1} Ce(III) ions onto XC beads at 300 K.